



CrossMark  
 click for updates

Cite this: *RSC Adv.*, 2015, 5, 105307

# An array of leaf-like $\text{Co}_3\text{Ni}$ microstructures with ferromagnetic properties, superhydrophobic properties and high catalytic performance in the hydrolysis of ammonia borane

Tao Zeng,<sup>a</sup> Jinyun Liao,<sup>b</sup> Hao Li,<sup>\*b</sup> Kejun Feng<sup>b</sup> and Liling Li<sup>c</sup>

In this work, a Cu foil supported array of leaf-like  $\text{Co}_3\text{Ni}$  microstructures composed of well aligned nanorods was synthesized by a facile electroless process. It was found that the as-prepared  $\text{Co}_3\text{Ni}$  array exhibited ferromagnetic properties with enhanced coercivity. The static contact angle of water on the surface of the  $\text{Co}_3\text{Ni}$  array could reach  $154.7^\circ$ , indicating that the  $\text{Co}_3\text{Ni}$  array displayed superhydrophobic properties. In addition, the as-prepared  $\text{Co}_3\text{Ni}$  array showed high catalytic activity in the hydrolysis of ammonia borane for hydrogen generation. More importantly, the  $\text{Co}_3\text{Ni}$  array catalyst still retained ca. 91% of its original catalytic activity after 6 cycles, exhibiting significantly improved recyclability and reusability in contrast to many nanocatalysts reported in the literature. The high catalytic performance, together with its ferromagnetic and superhydrophobic properties, makes the  $\text{Co}_3\text{Ni}$  array a multifunctional material with wide applications in different areas.

Received 28th October 2015  
 Accepted 30th November 2015

DOI: 10.1039/c5ra22621j

[www.rsc.org/advances](http://www.rsc.org/advances)

## Introduction

The worldwide energy consumption is sharply increasing and the current energy system based on fossil fuels is considered to be a major cause for global climate changes and environmental pollution. So, the development of sustainable, environment-friendly and cost-effective energy sources is undoubtedly the most important task in the 21st century. Owing to its high energy density, zero emission and as an abundant source, hydrogen is regarded as an ideal next-generation fuel.<sup>1,2</sup> Many techniques have been developed to produce and store hydrogen in the past few decades. In particular, generation of hydrogen *via* catalytic hydrolysis of chemical hydrides, such as  $\text{NaBH}_4$ ,  $\text{N}_2\text{H}_4$  and  $\text{NH}_3\text{BH}_3$  (ammonia borane, AB), has been extensively investigated in view of its high efficiency, convenience and safety.<sup>3–5</sup> Among these chemical hydrides, AB has the highest hydrogen storage capacity (19.6 wt%), which renders it more suitable for the application in the production/storage of hydrogen. In the catalytic hydrolysis of AB, catalyst is a key factor which will significantly affect the efficiency of hydrogen generation. In addition to noble metal catalysts, some low-cost catalysts, such as  $\text{Co}$ ,<sup>6,7</sup>  $\text{Co-B}$ ,<sup>8</sup>  $\text{Co-Mo-B-P}$ ,<sup>9</sup>  $\text{Ni}$ ,<sup>10</sup> also show relatively high catalytic activity in the AB hydrolysis. However,

these catalysts are usually unsupported nanoparticles or nanoparticles supported on powdery substrate, such as activated carbon,  $\text{Al}_2\text{O}_3$ , zeolite.<sup>11–13</sup> Obviously, those catalysts in the form of fine powder are prone to aggregate under the drive of high surface energy, which will reduce their active surface area and thus lower their catalytic activity.<sup>14</sup> Additionally, the tedious and costly separation and recovery procedure of the powdery nanocatalysts is another challenge when these catalysts are in industry-scale application. So, from a technological and operational point of view, it is highly expected to design low-cost catalysts with high stability, good recyclability, as well as high catalytic activity. On the other hand, hierarchical nano/microstructures have attracted increasing attention in recent years because of their excellent performance, enabled by their unique geometry and efficient charge transfer.<sup>15,16</sup> Generally speaking, hierarchical nano/microstructures are composed of numerous nanosized subunits, which are arranged in a specific manner. In the field of catalysis, it has been well verified in literature that the hierarchical nanostructures/microstructures exhibit high catalytic performance in many cases due to their special architectures.<sup>17,18</sup> However, hydrolysis of AB for hydrogen generation catalyzed by hierarchical nanostructures/microstructures has been seldom concerned.

In this work, an array of hierarchical leaf-like  $\text{Co}_3\text{Ni}$  microstructures supported on the Cu substrate was successfully prepared by a facile electroless approach. Compared with the traditional electro-deposition method for fabricating dendritic arrays of metals/alloys of iron group,<sup>19,20</sup> the synthetic process presented in this work is simple and cost-effective. The catalytic

<sup>a</sup>College of Environmental and Chemical Engineering, Shanghai University of Electric Power, Shanghai 200090, China

<sup>b</sup>Department of Chemical Engineering, Huizhou University, Huizhou, 516007, China. E-mail: lihao180@126.com; Fax: +86-752-2527229; Tel: +86-752-2527229

<sup>c</sup>Department of Pharmacy, Huizhou Health Sciences Polytechnic, Huizhou, 516007 China

performance of the as-prepared  $\text{Co}_3\text{Ni}$  array in the hydrolysis of AB is tested. As far as we know, an alloy of Co and Ni with similar microstructures in the form of an array has not been previously reported. Meanwhile, this is the first report on the AB hydrolysis for hydrogen generation catalyzed by hierarchical leaf-like  $\text{Co}_3\text{Ni}$  microstructures. Additionally, owing to its special microstructures, the as-prepared  $\text{Co}_3\text{Ni}$  array exhibits both ferromagnetic property and superhydrophobic property, making it a multifunctional material with wide applications in different fields.

## Experimental section

### Materials and synthesis

All reagents were of analytic grade, and double-distilled water was used throughout the experiments. To prepare the array of leaf-like  $\text{Co}_3\text{Ni}$  microstructures supported on Cu substrate, 1.5 mmol  $\text{CoCl}_2 \cdot 6\text{H}_2\text{O}$  and 0.5 mmol  $\text{NiCl}_2 \cdot 6\text{H}_2\text{O}$  was dissolved into 20 mL water under intense stirring, followed by the addition of 8 mmol triethylenetetramine and 2 mmol sodium dodecylsulfate to the mixed solution. Then, 10 mL NaOH (20 M), 10 mL hydrazine hydrate solution (50%) and 40 mL ethanol were dropped in sequence to the above solution. Afterwards, the mixture was quickly transferred into a Teflon-lined steel autoclave, in which a piece of 5 cm  $\times$  12 cm Cu foil with a thickness of *ca.* 10  $\mu\text{m}$  and a weight of  $0.54 \pm 0.02$  g (obtained from Guangzhou Great Power Energy & Technology CO., Ltd.) closely attached to the inner wall of vessel was used as support. Then the autoclave was put in the center of a circular column magnet with the magnetic field intensity of *ca.* 0.2 Tesla around the inner wall of the vessel. Finally, the autoclave, together with the magnet, was kept in an air oven at 120  $^\circ\text{C}$  for 8 h.

### Characterization

X-Ray diffraction (XRD) patterns were recorded using a PANalytical B. V. Empyeon X-ray diffractometer with Cu  $K\alpha$  radiation ( $\lambda = 1.5406$   $\text{\AA}$ ). The morphology of the array was investigated using a Hitachi S-4800 field emission scanning electron microscope (FE-SEM) equipped with an X-ray energy-dispersive spectrometer (EDS). Transmission electron microscopy (TEM) images were obtained on a JEOL JEM-2100 transmission electron microscope operated at 200 kV. The mass of Co and Ni deposited on the Cu foil was measured by a Varian 720 Inductively Coupled Plasma-Optical Emission Spectrometer (ICP-OES). The magnetic property of the sample was measured by a Quantum Design MPMS XL-7 superconducting quantum interference device magnetometer (SQUID). Contact angle was measured by a contact angle meter (OCA20, DataPhysics Instruments GmbH, Germany) at ambient temperature. The specific surface area was measured on a Quantachrome Autosorb-1 volumetric analyzer, using nitrogen adsorption and the Brunauer–Emmett–Teller method.

### Catalytic performance testing

The catalytic performance of the array of leaf-like  $\text{Co}_3\text{Ni}$  microstructures supported on Cu foil was assessed by

determining the accumulative volume of hydrogen generated during AB hydrolysis reaction in a glass reactor connected with a gas burette. In a typical procedure, 20 mL of freshly-prepared AB solution (0.2 M) was added in the reactor, followed by the addition of the  $\text{Co}_3\text{Ni}$  array supported on Cu foil (5 cm  $\times$  3 cm). The reaction temperature was fixed at  $308 \pm 0.5$  K in a thermostated reactor. The reusability of the  $\text{Co}_3\text{Ni}$  array was evaluated by repeating the hydrolysis reaction 6 times in such a model: (1) recollecting the catalyst after reaction; (2) washing the catalyst with water and ethanol alternatively before drying at 50  $^\circ\text{C}$  in vacuum oven; (3) starting a new run of AB hydrolysis by mixing the catalyst with freshly-prepared AB solution.

## Results and discussion

The crystal structures of the Cu substrate, as well as the Cu foil supported  $\text{Co}_3\text{Ni}$  array, are investigated by XRD and the results are shown in Fig. 1. It is observed that bare Cu substrate shows three characteristic peaks at  $2\theta = 43.4^\circ$ ,  $50.6^\circ$  and  $74.2^\circ$ , corresponding to the (111), (200) and (220) planes of face-centered cubic (fcc) phase of Cu (PDF#89-2838). Apart from these peaks, other three peaks at  $2\theta = 44.4^\circ$ ,  $51.6^\circ$  and  $76.1^\circ$  are observed in the XRD pattern of the Cu foil supported  $\text{Co}_3\text{Ni}$  array, which can be indexed to the diffractions from the (111), (200) and (220) planes of the fcc phase of CoNi alloy.<sup>21</sup>

Fig. 2a and b display the digital camera photos of the bare Cu foil and the Cu foil supported  $\text{Co}_3\text{Ni}$  array, respectively. As can be seen, the Cu foil is originally purple yellow in color and changes into gray black after the deposition of  $\text{Co}_3\text{Ni}$ . The morphology of the Cu supported  $\text{Co}_3\text{Ni}$  array, as well as the Cu foil, is analyzed by FE-SEM and the results are shown in Fig. 2c–f. Clearly, the bare Cu foil is relatively smooth on its surface (Fig. 2c). After the deposition of  $\text{Co}_3\text{Ni}$ , the surface becomes very coarse (Fig. 2d). Fig. 2e indicates that the  $\text{Co}_3\text{Ni}$  layer is composed of numerous leaf-like  $\text{Co}_3\text{Ni}$  microstructures, which are perpendicular to the Cu substrate. The high magnification SEM image in Fig. 2f displays the architecture of a piece of

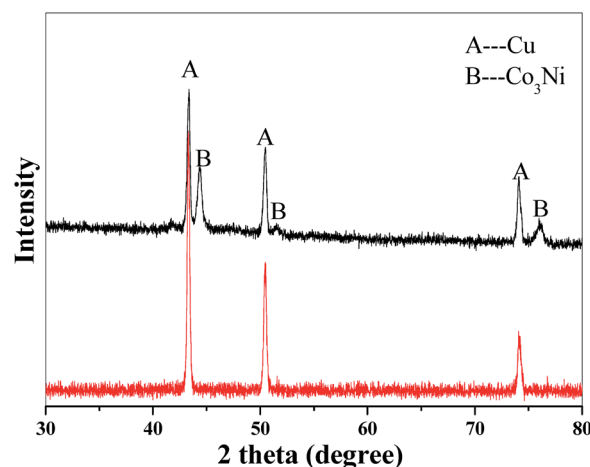


Fig. 1 XRD patterns of the Cu foil (a) and the Cu foil supported  $\text{Co}_3\text{Ni}$  array (b).

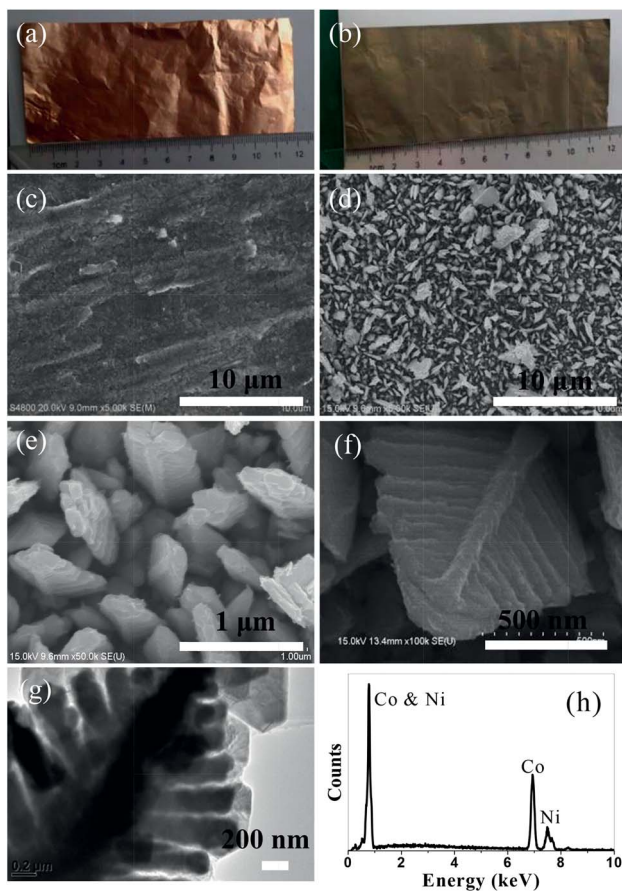


Fig. 2 Digital camera photos of the Cu foil (a) and the Cu foil supported  $\text{Co}_3\text{Ni}$  array (b); SEM images of the Cu foil (c) and the Cu foil supported  $\text{Co}_3\text{Ni}$  array (d–f); TEM image (g) and EDS pattern (h) of the  $\text{Co}_3\text{Ni}$  array.

$\text{Co}_3\text{Ni}$  leaf, which is consisting of a main stem with a diameter of 80–200 nm and many parallel rod-like branches with a diameter of *ca.* 150 nm on both sides of the stem. The TEM image in Fig. 2g further confirms the leaf-like structure of  $\text{Co}_3\text{Ni}$  in the array. It should be mentioned that even a 30 min ultrasonic treatment can not detach these  $\text{Co}_3\text{Ni}$  microstructures from the Cu substrate, implying that the as-prepared  $\text{Co}_3\text{Ni}$  array is very stable. The typical EDS pattern of a leaf-like  $\text{Co}_3\text{Ni}$  microstructure in Fig. 2h indicates the atomic ratio of Co to Ni is *ca.* 72 : 28. The ICP-OES analysis demonstrates the atomic ratio of Co to Ni is *ca.* 74 : 26. Both ratios are very close to the targeted composition of 3 : 1. According to the ICP-OES result, the mass of the  $\text{Co}_3\text{Ni}$  array deposited on Cu foil ( $5 \times 12$  cm) is *ca.* 36.4 mg, and the corresponding catalyst loading on Cu foil is  $0.61 \text{ mg cm}^{-2}$ .

In this study,  $\text{Co}_3\text{Ni}$  alloy was produced by the co-reduction of  $\text{Co}^{2+}$  and  $\text{Ni}^{2+}$ . At the early stage of the reduction process, plentiful primary  $\text{Co}_3\text{Ni}$  alloy nuclei are formed in solution, which will be magnetized and migrate to the Cu substrate under the magnetic force provided by the external magnet. After they are deposited on the Cu foil, these nuclei will act as crystal nuclei and provide heterogeneous nucleation sites for crystal

growth. As the reduction reaction proceeds, more and more  $\text{Co}_3\text{Ni}$  clusters will be formed and move to the Cu substrate, then add themselves to existing nuclei. In such model, nanostructures on the Cu substrate are formed.

To determine the magnetic properties of the Cu supported array of leaf-like  $\text{Co}_3\text{Ni}$  microstructures, magnetic measurements at 298 K were carried out on the array, with the applied field parallel and vertical to the Cu substrate. The magnetic hysteresis loops are displayed in Fig. 3, which demonstrate the array has typical ferromagnetic properties. When the applied external magnetic was parallel to the Cu substrate, the saturation magnetization, the remnant magnetization and the coercivity of the array is  $114.0 \text{ emu g}^{-1}$ ,  $58.8 \text{ emu g}^{-1}$  and  $79.5 \text{ Oe}$ , respectively. While when the applied external magnetic was vertical to the Cu substrate, the saturation magnetization, the remnant magnetization and the coercivity of the array is  $96.7 \text{ emu g}^{-1}$ ,  $11.1 \text{ emu g}^{-1}$  and  $286.8 \text{ Oe}$ , respectively. Compared with the coercivity of the nanosized  $\text{Co}_{75}\text{Ni}_{25}$  alloy ( $31.69 \text{ Oe}$ ),<sup>22</sup> our  $\text{Co}_3\text{Ni}$  array exhibits much higher coercivity. It has been demonstrated that a nonspherical nanosized magnetic materials can possess shape anisotropy and a small departure from sphericity in shape will cause a significant increase of coercivity.<sup>23</sup> In the present study, the shape anisotropy of the leaf-like  $\text{Co}_3\text{Ni}$  microstructures may be responsible for the improved coercivity.

To evaluate the wettability of the  $\text{Co}_3\text{Ni}$  array, the static contact angle was determined. Fig. 4 is the typical photograph of a water droplet on the Cu supported  $\text{Co}_3\text{Ni}$  array. The contact angle of the  $\text{Co}_3\text{Ni}$  array is  $154.7^\circ$ , indicating that the  $\text{Co}_3\text{Ni}$  array exhibit superhydrophobic property. It is known that the superhydrophobic materials can be obtained by the construction of appropriate surface hierarchical micro/nanostructures and chemical composition.<sup>24</sup> As far as our sample concerned, the leaf-like  $\text{Co}_3\text{Ni}$  microstructures in the array consist of well aligned nanorods. Such hierarchical micro/nanostructures on the surface of the Cu substrate account for the superhydrophobic properties of the sample.

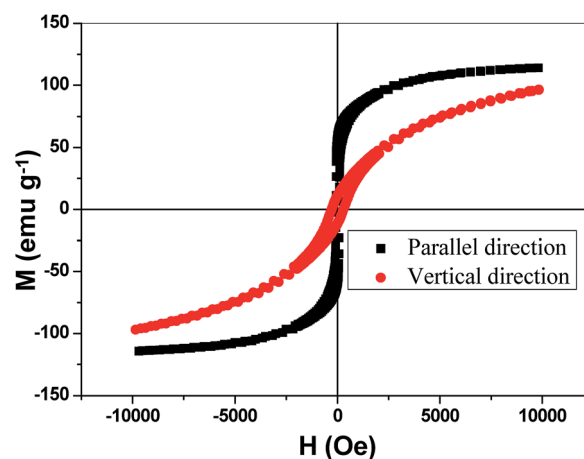


Fig. 3 Magnetic hysteresis loops of the Cu foil supported  $\text{Co}_3\text{Ni}$  array with the applied external magnetic field parallel and vertical to the Cu substrate.

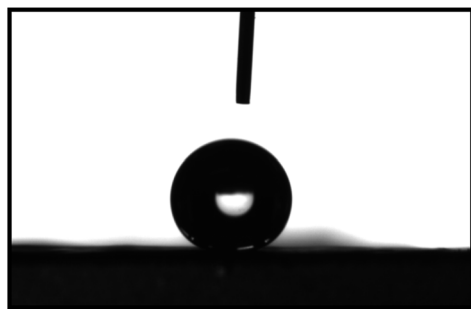


Fig. 4 Typical photograph of a water droplet on the surface of Cu foil supported  $\text{Co}_3\text{Ni}$  array.

In the present study, the as-prepared Cu foil supported array of leaf-like  $\text{Co}_3\text{Ni}$  microstructures as a catalyst for the hydrolysis of AB is investigated. To clarify the role of Cu substrate, hydrolysis of AB in the presence of bare Cu foil is carried out. It is found that nearly no hydrogen is generated, suggesting that the Cu foil in our work has no catalytic activity in the hydrolysis reaction. In contrast, when the array of leaf-like  $\text{Co}_3\text{Ni}$  microstructures acts as a catalyst, hydrogen is continuously generated. Fig. 5 shows the relationship of the accumulated volume of hydrogen vs. reaction time at different catalyst dosages in terms of geometrical surface areas of film catalyst, which are the product of the length and the width of the film. As can be observed, the accumulated volume of hydrogen is directly proportional to the reaction time, hinting that the hydrolysis of AB catalyzed by the  $\text{Co}_3\text{Ni}$  array is zero-order with respect to the concentration of AB. This implies that the adsorption of AB on the array surface may be a rate-limiting step.<sup>25</sup> Noting that the volume of hydrogen at the late stage of the hydrolysis (after 20 min) is smaller than the normal value at catalyst dosages of 22.5 and 30.0  $\text{cm}^2$ . Similar results have also been reported by other groups.<sup>8,10</sup> The corresponding rate constants can be calculated from the slopes of fitting lines in Fig. 5 and the results are listed in Table 1. The total turnover frequency (TOF) of catalyst

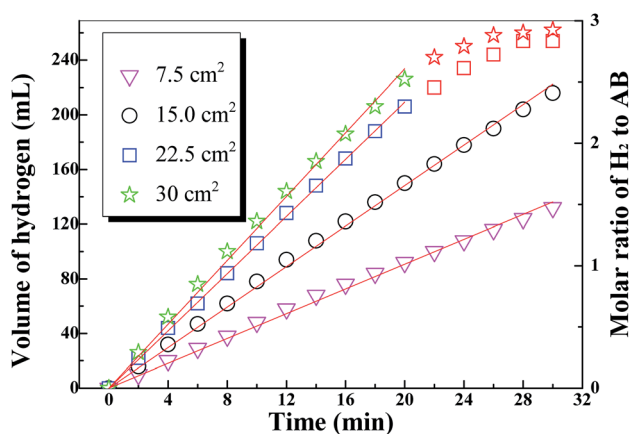


Fig. 5 Accumulative volume of hydrogen generated during AB hydrolysis vs. reaction times at different catalyst dosages in terms of geometrical surface ( $T = 308$  K).

Table 1 Comparison of rate constants and BET surface normalized rate constants of AB hydrolysis when  $\text{Co}_3\text{Ni}$  array and  $\text{Co}_3\text{Ni}$  nanoparticles act as catalysts

Catalyst dosage	Rate constant ( $\text{mL min}^{-1}$ )		BET surface area normalized rate constant ( $\text{mL min}^{-1} \text{m}^2$ )	
	$\text{Co}_3\text{Ni}$ array	$\text{Co}_3\text{Ni}$ nanoparticles	$\text{Co}_3\text{Ni}$ array	$\text{Co}_3\text{Ni}$ nanoparticles
4.6 mg	4.5	3.3	72.5	32.8
9.1 mg	7.4	4.8	60.2	24.1
13.7 mg	10.5	6.6	56.8	22.0
18.4 mg	11.7	7.2	47.1	17.9

can also be calculated based on these data. At catalyst dosage of 9.1 mg, the value of TOF is *ca.*  $2.03 \text{ mol H}_2 \text{ min}^{-1} (\text{mol cat.})^{-1}$ .

It is worth noting that production of hydrogen *via* AB hydrolysis catalyzed by various catalysts has been widely reported and a huge number of data on the rate constants of AB hydrolysis have been published in literature. However, the detailed reaction conditions of AB hydrolysis, such as reaction model, reaction temperature, catalyst dosage, concentration of AB and even the support, are not the same in different reports. So, it may be unsound to assess these catalysts by comparing their rate constants or TOF without normalizing these parameters. In this study, for comparison,  $\text{Co}_3\text{Ni}$  nanoparticles with a diameter of 40–50 nm synthesized by a modified polyol method<sup>26</sup> instead of the leaf-like  $\text{Co}_3\text{Ni}$  array were used as a catalyst while other reaction conditions were kept the same. The corresponding results are also shown in Table 1. As can be seen, our  $\text{Co}_3\text{Ni}$  array exhibit higher catalytic activity than  $\text{Co}_3\text{Ni}$  nanoparticles in the hydrolysis of the AB. Two possible reasons account for the fact that the  $\text{Co}_3\text{Ni}$  array shows much higher catalytic activity than  $\text{Co}_3\text{Ni}$  nanoparticles. Firstly,  $\text{Co}_3\text{Ni}$  layers supported on substrate are composed of shape-anisotropic leaf-like microstructures, which have more corners and edges than the spherical nanoparticles. Generally, the atoms on the corners or edges have unsaturated valency with less number of bonds around them than those in the interiors or on the faces.<sup>27</sup> Such atoms have much higher intrinsic catalytic activity. In this study, the BET surface areas of  $\text{Co}_3\text{Ni}$  array and the  $\text{Co}_3\text{Ni}$  nanoparticles were measured, which were 13.5 and 21.9  $\text{m}^2 \text{g}^{-1}$ , respectively. Correspondingly, the BET surface area normalized rate constants can be figured out. As shown in Table 1, BET surface area normalized rate constants of  $\text{Co}_3\text{Ni}$  array is significantly larger than those of  $\text{Co}_3\text{Ni}$  nanoparticles, hinting that  $\text{Co}_3\text{Ni}$  array has higher intrinsic catalytic activity than  $\text{Co}_3\text{Ni}$  nanoparticles. Secondly, these  $\text{Co}_3\text{Ni}$  nanoparticles suspended in AB solution during hydrolysis reaction tend to agglomerate due to their high surface energy, as well as the magnetic attraction among the  $\text{Co}_3\text{Ni}$  nanoparticles resulted from their ferromagnetic property.<sup>14</sup> In this case, the surface area of particulate  $\text{Co}_3\text{Ni}$  catalyst will decrease, resulting in the decline of catalytic performance. In contrast, the leaf-like  $\text{Co}_3\text{Ni}$  microstructures in the array are immobilized on the surface of

substrate and therefore the decrease of catalytic activity related to the aggregation is evitable.

The apparent activated energy ( $E_a$ ) is a very important parameter of a catalyst, which can be applied to evaluate its catalytic performance. In general, a catalyst with lower activation energy in the catalytic reaction always shows a higher catalytic activity. In this study, the hydrolysis of AB catalyzed by the  $\text{Co}_3\text{Ni}$  array was carried out at various temperatures to obtain the  $E_a$  value. As displayed in Fig. 6a, the hydrolysis of AB is enhanced as the reaction temperature increases. The hydrolysis rate is 5.0, 7.4, 10.5 and 19.4  $\text{mL min}^{-1}$  at reaction temperature of 298 K, 308 K, 318 K and 328 K, respectively. On the basis of these data,  $E_a$  of the AB hydrolysis catalyzed by the leaf-like  $\text{Co}_3\text{Ni}$  array can be calculated according to the classical Arrhenius equation, which is 35.6  $\text{kJ mol}^{-1}$  (Fig. 6b). This value is higher than that of  $\text{Co}_{35}\text{Pd}_{65}/\text{C}$  catalyst (27.5  $\text{kJ mol}^{-1}$ )<sup>25</sup> and Co-P catalyst (22  $\text{kJ mol}^{-1}$ ),<sup>28</sup> but is significantly lower than those of recently reported Co-based and Ni-based catalysts, such as Co/ $\gamma$ - $\text{Al}_2\text{O}_3$  (62  $\text{kJ mol}^{-1}$ ),<sup>11</sup> Co/zeolite (56  $\text{kJ mol}^{-1}$ ),<sup>13</sup> PVP-Co (46  $\text{kJ mol}^{-1}$ )<sup>29</sup> and  $\text{Co}_{0.75}\text{B}_{0.25}$  (40.85  $\text{kJ mol}^{-1}$ ),<sup>30</sup> bulk Ni (70  $\text{kJ mol}^{-1}$ ),<sup>31</sup> CoNi/RGO (39.89  $\text{kJ mol}^{-1}$ )<sup>32</sup> and  $\text{Ni}_{0.97}\text{Pt}_{0.03}$  (57  $\text{kJ mol}^{-1}$ ).<sup>33</sup>

The reusability and durability of a catalyst are important concerns to be considered before its practical applications. In

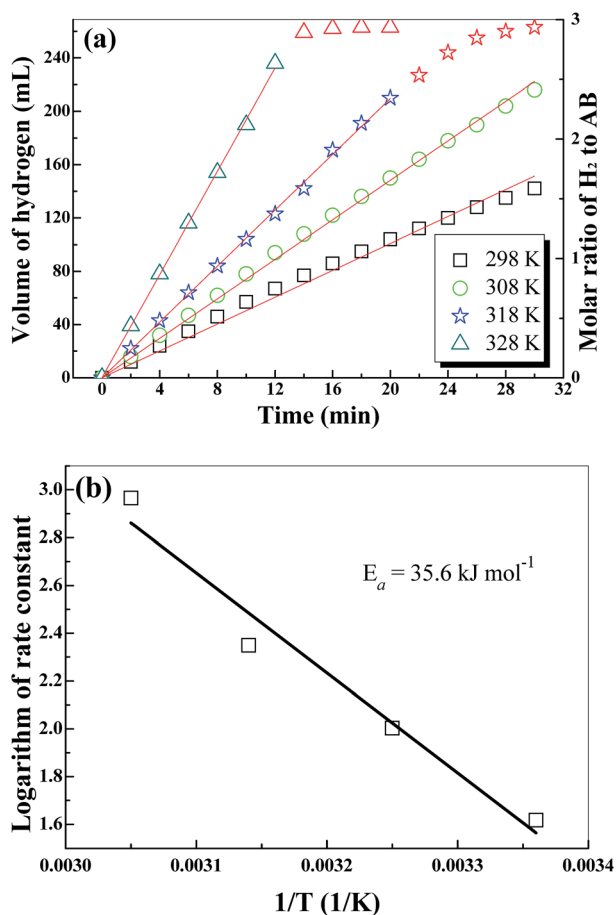


Fig. 6 (a) Accumulative volume of hydrogen generated during AB hydrolysis vs. reaction times at different reaction temperatures; (b) the logarithm of rate constants vs. reciprocal of reaction temperature.

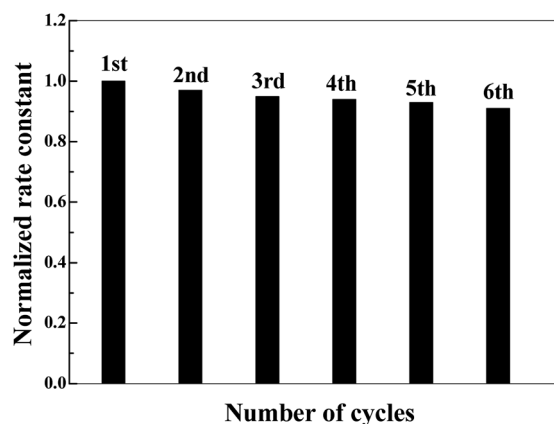


Fig. 7 Normalized rate constant at different cycles.

this work, the normalized rate constant, *i.e.*  $k_n/k_1$ , where  $k_1$  and  $k_n$  represents respectively the rate constant of AB hydrolysis in cycle 1 and cycle  $n$ , is applied to assess the durability and reusability of the as-prepared array of leaf-like  $\text{Co}_3\text{Ni}$  microstructures supported on the Cu foil. As can be observed in Fig. 7, the normalized rate constant is as high as 0.91 after 6 cycles, indicating that the used catalyst still retains *ca.* 91% catalytic activity of its original activity. In contrast, the  $\text{Co}_3\text{Ni}$  nanoparticles obtained *via* the modified polyol method lose *ca.* 40% activity after 6 cycles. Moreover, the as-prepared Cu supported array of leaf-like  $\text{Co}_3\text{Ni}$  microstructures also exhibits much better durability and reusability than many Co or Co-containing nanocatalysts in literature, such as intrazeolite Co nanoclusters (31% activity loss in the fifth run),<sup>13</sup> CoNi/RGO (31% activity loss in the fifth run).<sup>32</sup> For those Co or Co-containing nanocatalysts in the form of powder, the material loss during the process of separation, drying and re-dispersed is a common reason that causes the decrease in the activity of the catalysts.<sup>13</sup> Also, under the drive of high surface energy and the attraction of magnetic force among each other, the fine powdery particles are very likely to aggregate during the process of usage, isolation and desiccation, which will result in a remarkable loss of the catalytic activity in the long-term run. In contrast, the leaf-like  $\text{Co}_3\text{Ni}$  microstructures in the array are immobilized on the Cu foil, so



Fig. 8 SEM image of the  $\text{Co}_3\text{Ni}$  array after 6 cycles.

the activity drop caused by the migration and aggregation of Co<sub>3</sub>Ni microstructures is evitable. Besides, the alteration of shapes and morphology of micro- or nanocatalysts during catalytic process can also influence their catalytic performance.<sup>34</sup> To clarify this, the SEM image of the Co<sub>3</sub>Ni array catalyst after 6 cycles are shown in Fig. 8, demonstrating that there is no remarkable morphology change in the Co<sub>3</sub>Ni array. This observations hint that the Co<sub>3</sub>Ni array is stable under our experiment conditions.

## Conclusions

In summary, an array of leaf-like Co<sub>3</sub>Ni microstructures supported on the Cu foil was prepared, which showed high catalytic activity in the hydrolysis of AB. The apparent activated energy of the AB catalyzed by the as-prepared Co<sub>3</sub>Ni array was calculated to be ca. 35.6 kJ mol<sup>-1</sup>, which is much lower than those of many Co-based and Ni-based nanocatalyst in literature. Also, it displayed better durability and reusability in contrast to many powdery Co-based nanocatalysts. Owing to its high catalytic activity, good durability and reusability, as well as the low cost, the array of leaf-like Co<sub>3</sub>Ni microstructures showed great potential in the applications in the hydrolysis of ammonia borane for hydrogen generation. In addition, the as-prepared Co<sub>3</sub>Ni array exhibits both ferromagnetic property and superhydrophobic property due to its special architecture, which make it a multifunctional material with wide applications in different fields.

## Acknowledgements

This work was financially supported by the Science and Technology Commission of Shanghai Municipality (No. 14DZ2261000), the National Natural Science Foundation of China (No. 51001052), the High-level Talent Project of the University in Guangdong Province (184), the Distinguished Young teachers in Higher Education of Guangdong Province (No. Yq2013154), and the Characteristic and Innovative Project of the Education Department of Guangdong Province (No. 2014KTSCX177).

## Notes and references

- 1 J. A. Turner, *Science*, 2004, **305**, 972–974.
- 2 Z.-M. Huang, A. Su and Y.-C. Liu, *Energy*, 2013, **51**, 230–236.
- 3 G. H. Liu and Z. P. Li, *J. Power Sources*, 2009, **187**, 527–534.
- 4 W. Chen, J. Ji, X. Duan, G. Qiang, P. Li, X. Zhou, D. Chen and W. Yuan, *Chem. Commun.*, 2014, **50**, 2142–2144.
- 5 L. He, Y. Huang, X. Y. Liu, L. Li, A. Wang, X. Wang, C.-Y. Mou and T. Zhang, *Appl. Catal., B*, 2014, **147**, 779–788.
- 6 M. Paladini, G. M. Arzac, V. Godinho, M. C. Jiménez De Haro and A. Fernández, *Appl. Catal., B*, 2014, **158–159**, 400–409.
- 7 J. Liao, H. Li and X. Zhang, *Catal. Commun.*, 2015, **67**, 1–5.
- 8 N. Patel, R. Fernandes, G. Guella and A. Miotello, *Appl. Catal., B*, 2010, **95**, 137–143.
- 9 R. Fernandes, N. Patel, A. Miotello and L. Calliari, *Top. Catal.*, 2012, **55**, 1032–1039.
- 10 M. Mahyari and A. Shaabani, *J. Mater. Chem. A*, 2014, **2**, 16652–16659.
- 11 Q. Xu and M. A. Chandra, *J. Alloys Compd.*, 2007, **446–447**, 729–732.
- 12 Q. Xu and M. Chandra, *J. Power Sources*, 2006, **163**, 36–370.
- 13 M. Rakap and Ö. Saim, *Int. J. Hydrogen Energy*, 2010, **35**, 3341–3346.
- 14 Y. Du, H. Chen, R. Chen and N. Xu, *Appl. Catal., A*, 2004, **277**, 259–264.
- 15 J. Bai, X. Li, G. Liu, Y. Qian and S. Xiong, *Adv. Funct. Mater.*, 2014, **24**, 3012–3020.
- 16 M. U. Anu Prathap, S. Sun, C. Wei and Z. J. Xu, *Chem. Commun.*, 2015, **51**, 4376–4379.
- 17 C. Deng, X. Ge, H. Hu, L. Yao, C. Han and D. Zhao, *CrystEngComm*, 2014, **16**, 2738–2745.
- 18 M. Wang, T. Sun, Y. Shi, G. Jiang and Y. Tang, *CrystEngComm*, 2014, **16**, 10624–10630.
- 19 K. H. Kim, J. Y. Zheng, W. Shin and Y. S. Kang, *RSC Adv.*, 2014, **2**, 4759–4767.
- 20 J. Y. Zheng, Z. L. Quan, G. Song, C. W. Kim, H. G. Cha, T. W. Kim, W. Shin, K. J. Lee, M. H. Jung and Y. S. Kang, *J. Mater. Chem.*, 2012, **22**, 12296–12304.
- 21 H. Li, J. Liao, Y. Feng, S. Yu, X. Zhang and Z. Jin, *CrystEngComm*, 2012, **14**, 2974–2980.
- 22 M. Shen, Y.-F. Wang, F. Zhang and Q.-S. Wu, *J. Phys. Chem. C*, 2009, **113**, 5960–5966.
- 23 D. L. Leslie-Pelecky and R. D. Rieke, *Chem. Mater.*, 1996, **8**, 1770–1783.
- 24 K. Liu and L. Jiang, *Nanoscale*, 2011, **3**, 825–838.
- 25 D. Sun, V. Mazumder, Ö. Metin and S. Sun, *ACS Nano*, 2011, **5**, 6458–6464.
- 26 J. Bregado-Gutiérrez, A. J. Saldívar-García and H. F. Lopez, *Mater. Lett.*, 2008, **62**, 939–942.
- 27 M. A. Mahmoud, F. Saira and M. A. El-Sayed, *Nano Lett.*, 2010, **10**, 3764–3769.
- 28 K. S. Eom, K. W. Cho and H. S. Kwon, *Int. J. Hydrogen Energy*, 2010, **35**, 181–186.
- 29 Ö. Metin and S. Özkaz, *Energy Fuels*, 2009, **23**, 3517–3526.
- 30 A. K. Figen, *Int. J. Hydrogen Energy*, 2013, **38**, 9186–9197.
- 31 S. B. Kalidindi, M. Indirani and B. R. Jagirdar, *Inorg. Chem.*, 2008, **47**, 7424–7429.
- 32 Y. Yang, F. Zhang, H. Wang, Q. Yao, X. Chen and Z.-H. Lu, *J. Nanomater.*, 2014, **2014**, 1–9.
- 33 F. Cheng, H. Ma, Y. Li and J. Chen, *Inorg. Chem.*, 2007, **43**, 788–794.
- 34 X. Liu, D. Wang and Y. Li, *Nano Today*, 2012, **7**, 448–466.